NASA Contractor Report 158986

STRESSES IN A THREE-DIMENSIONAL UNIDIRECTIONAL COMPOSITE CONTAINING BROKEN FIBERS

James G. Goree and Robert S. Gross

CLEMSON UNIVERSITY
Department of Mechanical Engineering
College of Engineering
Clemson, SC 29631

NASA Grant NSG-1297
October 1978

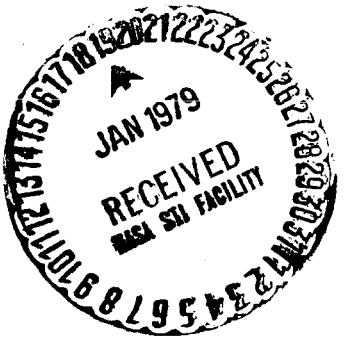

National Aeronautics and
Space Administration

Langley Research Center
Hampton, Virginia 23665

ANNUAL REPORT NASA GRANT NSG-1297

STRESSES IN A THREE-DIMENSIONAL UNIDIRECTIONAL COMPOSITE CONTAINING BROKEN FIBERS

Principal Investigator

James G. Goree
Professor of Mechanics and
Mechanical Engineering

Graduate Assistant

Robert S. Gross
M.S. Candidate in Engineering Mechanics

ABSTRACT

An approximate solution is developed for the determination of the interlaminar normal and shear stresses in the vicinity of a crack in a three dimensional composite containing unidirectional linearly elastic fibers in an infinite linearly elastic matrix.

In order to reduce the complexity of the formulation, certain assumptions are made as to the physically significant stresses to be retained. These simplifications reduce the partial differential equations of elasticity to differential-difference equations which are tractable using Fourier transform techniques. This "material modeling" approach is in contrast with solutions developed by considering each lamina as a homogeneous, orthotropic layer. The resulting solution does not contain the classical singular stress field for the fibers and the influence of broken fibers on unbroken fibers is felt by a change in stress concentration factors. The matrix stresses however, are unbounded as the fiber spacing vanishes and an equivalent fiber-matrix geometry is proposed which gives the correct singular behavior.

The numerical solution is considered in detail and several specific examples are presented. The potential for damaged or debonded zones to be generated by an embedded crack is discussed, and stress concentration factors for fibers near the crack are given. Detailed comparisons are made between the present solution, the analogous two-dimensional problem, and corresponding shear-lag models.

TABLE OF CONTENTS

LIST OF TABLES

LIST OF FIGURES

LIST OF SYMBOLS

A_F, b	Fiber cross-sectional area and fiber diameter or width respectively.
A_i, B_i, C_i, D_i	Functions of (θ,ϕ), $i = 1,2,3$, see equations (27), (28), (29).
E_F, E_M, G_M	Young's moduli of the fiber and matrix and the shear modulus of the matrix respectively.
$\overline{E}_F$, $\overline{E}_M$	Normalized moduli, $\overline{E}_F = E_F/G_M$, $\overline{E}_M = E_M/G_M$.
$H_{r,s}$	Constants specified by equation (48).
h	Shear transfer length, See Figures 6 and 7.
$u_{m,n}$, $v_{m,n}$, $w_{m,n}$	x, y, and z components of displacements. Functions of the axial coordinate x.
$U_{m,n}$, $V_{m,n}$, $W_{m,n}$	Normalized displacements, $(u_{m,n}/h, v_{m,n}/h, w_{m,n}/h)$.
$\overline{U}$, $\overline{V}$, $\overline{W}$	Transformed displacements, functions of (η, θ, ϕ), see equations (18), (19), and (20).
V_F	Fiber volume fraction
x, y, z	Cartesian coordinates
α_i	Coefficients given by equations (33), (34), and (35) $i = 1,4$. Functions of (θ,ϕ).
β_i	Coefficients given by equations (45) and (46), $i = 2,3$. Functions of (θ,ϕ).
γ	$\gamma = A_F/h^2$, see Figures 6 and 7.
θ,ϕ	Fourier Transform variables, see equations (18) - (23).
δ	Minimum spacing between fibers.
$\sigma_{x\ m,n}$	Axial stress in the m, n fiber, function of the axial coordinate x.
$\sigma_y\|_{m,n}$, $\sigma_z\|_{m,n}$, $\tau_{xy\ m,n}$, $\tau_{zy}\|_{m,n}$	Normal and shear stresses in the matrix between the m,n and m-1,n fibers and the m,n and m,n-1 fibers respectively.
$\overline{\sigma}_x$, $\overline{\sigma}_y$, $\overline{\sigma}_z$, $\overline{\tau}_{xy}$, $\overline{\tau}_{xz}$	Normalized stresses: σ_x/E_F, σ_y/E_F, σ_z/E_F, τ_{xy}/E_F, τ_{xz}/E_F.

STRESSES IN A THREE-DIMENSIONAL UNIDIRECTIONAL COMPOSITE CONTAINING BROKEN FIBERS

By

James G. Goree
Professor of Mechanics and
Mechanical Engineering, Clemson University
Clemson, South Carolina 29631

and

Robert S. Gross
Graduate Assistant, Department of
Mechanical Engineering, Clemson University
Clemson, South Carolina 29631

INTRODUCTION

In investigations concerning the potential use of composite materials in advanced structures, considerable attention has been given to problems associated with damage or flaws in laminates and to the resulting fatigue and fracture characteristics of the composite. The need for the capability to design damage tolerant composite structures with at least the same degree of confidence as now exists for metallic structures is essential if such materials are to be used in production.

For composite laminates, the technique of hybrid material buffer strips embedded at regular intervals throughout the laminate has been demonstrated, for example see [1], to have the capability of arresting through-the-laminate cracks, and in some cases to give a residual strength approaching the net section capacity of the laminate. The mechanism associated with the crack arrest and ultimate failure of such laminates has not, however, been explained nor have satisfactory methods been developed to allow for accurate prediction of crack arrest loads or ultimate failure in terms of the laminate geometry and materials. It does appear however, both from [1] and the experimental results reported in [2] that, for composite laminates containing embedded hybrid buffer strips or for single material laminates with weakened interface bonds, delamination between laminae appears to be directly associated with the laminates ability to restrict crack growth.

The panel containing embedded buffer strips is considerably different than the related design where either bonded or riveted stringers are added externally without significantly interrupting the continuity of the basic panel. The panel and stringers then act much more independently during

crack growth and fracture than appears to be the case in composite laminates with internal buffer strips. A detailed investigation of the problem of riveted stringers reinforcing a cracked isotropic elastic sheet is presented in [3]. Similar studies for adhesively bonded external stringers are reported in [4] and [5]. An analogous study concerning composite laminates with internal buffer strips has not, to the knowledge of the authors, been completed.

Considerable analytical work has been done for both isotropic and orthotropic materials in investigating the stresses in the vicinity of a crack tip for the crack being near, at, crossing, or along a material interface. (See [6], [7], [8], [9], [10], and [11].) These studies considered the laminate as a thin homogeneous isotropic or orthotropic plane and investigated the resulting two-dimensional stress state. Through the thickness variations in material properties and stresses were not considered. It appears that for the embedded hybrid buffer strip the significant stresses are, in fact, the interlaminar stresses and the three-dimensional problem must be considered. It does not seem reasonable to anticipate the development of a general solution in the manner of the above mentioned two-dimensional studies, as the extension to a three-dimensional stress state with finite thickness would be exceedingly complicated.

Some possibility of success might be had in modeling the laminate as in classical lamination theory, where, as discussed in [12] and [13], the interlaminar stresses near a free edge of a laminate have been approximated. Finite element or finite difference solutions also are a possibility; however, without some improvements in the current three-dimensional programs to account for through-the-thickness variations, the computation time seems prohibitive. A different approach, which appears to have more potential, is

to model the laminate as a heterogeneous material consisting of separate fiber and matrix phases, each with its own characteristic properties. If the proper assumptions are made regarding the dominant stresses carried by each phase, the appropriate field equations can be simplified considerably while still retaining the fundamental nature of the solution. One major assumption usually made in such a model is to neglect the normal stress in the matrix parallel to the fibers. The resulting solution then does not contain the classical singular stress field at the end of the notch but rather, the fibers feel the influence of the size of the notch as a change in a stress concentration factor.

Zweben in [14] presents a detailed discussion of this "material modeling" approach and in [14] and [15] a two-dimensional problem for a notched unidirectional laminate containing a damaged region with and without constraint respectively, is considered.

An earlier use of this technique was considered by Hedgepeth [16] and Hedgepeth and Van Dyke [17] for unidirectional fibers in a two-dimensional and three-dimensional array respectively. In each case however, the matrix was assumed to transmit only shear stresses and both studies reduced to one-dimensional solutions. Eringen and Kim, [18] extended the Hedgepeth model to include normal stresses in the matrix and investigated the two-dimensional problem of equally spaced parallel fibers in a single layer.

The present paper extends the method [16], [17], and [18] to the case of an arbitrary number of broken fibers in a three-dimensional composite containing equally spaced unidirectional fibers. The model developed below is basically the same as [18] with some difference in the equilibrium equation perpendicular to the fibers and the significant difference of the three-dimensional geometry.

Of course, the solution needed is for a finite thickness laminate containing angle-ply laminae, each of possibly different material properties than the adjacent laminae as well as allowing for different materials within a particular lamina. It is hoped that the present study will give some insight into the behavior of interlaminar stresses near a notch and aid in the development of more complete models. The extension of this investigation to include angle-ply laminae is currently being considered by the writers.

FORMULATION

Consider an infinite three-dimensional matrix containing parallel reinforcing fibers as indicated in Figure (1), where both the fibers and the matrix are assumed to be linearly elastic. The development given below will be restricted to identical parallel fibers with the spacing between fibers taken as equal. It is assumed that the fibers carry only normal stresses and, in fact, support all the normal stress in the composite in the direction parallel to the fibers. The matrix supports shear stresses parallel to the fibers and normal stresses perpendicular to the fibers. Using the coordinate system given in Figure (1), a typical element can be isolated as shown in Figure (2), where a particular fiber or matrix interface is identified by the indices m and n. Note that the composite is doubly periodic in the y, z plane; however, this symmetry is initially not required of the solution and random fibers may be taken as broken with rhe resulting solution having no symmetry in the y, z plane. All fiber breaks are assumed, however, to occur on the plane x = 0 so symmetry does exist with respect to this plane. The reduction to the special case of broken fibers which are symmetric to the y, z axes is covered following the general development and a considerable reduction in computation time is realized.

The equilibrium equations for the element shown in Figures (2) and (3) are

$$A_F \frac{d\sigma_x\Big|_{m,n}}{dx} + h\{\tau_{xy}\Big|_{m+1,n} - \tau_{xy}\Big|_{m,n}\} + h\{\tau_{xz}\Big|_{m,n+1} - \tau_{xz}\Big|_{m,n}\} = 0, \qquad (1)$$

$$\sigma_y\Big|_{m+1,n} - \sigma_y\Big|_{m,n} + \frac{h}{2}\frac{d}{dx}\{\tau_{xy}\Big|_{m+1,n} + \tau_{xy}\Big|_{m,n}\} = 0, \text{ and} \tag{2}$$

$$\sigma_z\Big|_{m,n+1} - \sigma_z\Big|_{m,n} + \frac{h}{2}\frac{d}{dx}\{\tau_{xz}\Big|_{m,n+1} + \tau_{xz}\Big|_{m,n}\} = 0. \tag{3}$$

The stress-strain and strain-displacements relations are approximated as follows, using the geometry of Figures (4) and (5).

$$\sigma_x\Big|_{m,n} = E_F \frac{du_{m,n}}{dx}, \tag{4}$$

$$\sigma_y\Big|_{m+1,n} = \frac{E_M}{h}\{v_{m+1,n} - v_{m,n}\}, \tag{5}$$

$$\sigma_z\Big|_{m,n+1} = \frac{E_M}{h}\{w_{m,n+1} - w_{m,n}\}, \tag{6}$$

$$\tau_{xy}\Big|_{m+1,n} = G_M\{\frac{1}{2}\frac{d}{dx}[v_{m+1,n} + v_{m,n}] + \frac{1}{h}[u_{m+1,n} - u_{m,n}]\}, \text{ and} \tag{7}$$

$$\tau_{xz}\Big|_{m,n+1} = G_M\{\frac{1}{2}\frac{d}{dx}[w_{m,n+1} + w_{m,n}] + \frac{1}{h}[u_{m,n+1} - u_{m,n}]\}. \tag{8}$$

In the above equations $u_{m,n}$, $v_{m,n}$, and $w_{m,n}$ are the x, y, and z components of the displacement of a point on the m,n fiber located a distance x from the y,z plane. The stress $\sigma_x\Big|_{m,n}$ is the axial stress in the fiber and the stresses $\sigma_y\Big|_{m,n}$, $\sigma_z\Big|_{m,n}$, $\tau_{xy}\Big|_{m,n}$, $\tau_{xz}\Big|_{m,n}$ are normal and shear stresses in the matrix. The constants E_F, E_M, and G_M are Young's moduli of the fiber and the

matrix and the shear modulus of the matrix respectively. A_F is the area of the fiber, and h is the shear transfer length.

The boundary conditions are for an infinite region, uniformly stressed at points remote to the mid-plane (y,z plane) containing an arbitrary number of broken fibers with the cracks always being at the mid-plane. Superposition may be used to consider two separate problems: the first, an infinite region containing no broken fibers and having a uniform axial stress, σ_o, in the fibers, and the second, the infinite region with no stresses at infinity and a compression stress of magnitude, σ_o, acting on the fibers at the cracks. The second problem will be considered below as it is the portion of the complete solution which is non-trivial.

The boundary conditions are then

$$u_{m,n} = v_{m,n} = w_{m,n} = 0 \qquad \text{for } x = \infty, \tag{9}$$

$$u_{m,n} = 0 \quad \text{for all unbroken fiber at } x = 0, \tag{10}$$

$$\sigma_x\big|_{m,n} = -\sigma_o \qquad \text{for all broken fibers at } x = 0, \tag{11}$$

$$\tau_{xy}\big|_{m,n} = 0 \qquad \text{for all fibers at } x = 0 \tag{12}$$

$$\tau_{xz}\big|_{m,n} = 0 \qquad \text{for all fibers at } x = 0 \tag{13}$$

The inclusion of the normal stresses in the matrix gives the necessary freedom to require equations (12) and (13). The above equations are normalized by letting

$$\eta = x/h, \quad U_{m,n} = u_{m,n}/h, \quad V_{m,n} = v_{m,n}/h, \quad W_{m,n} = w_{m,n}/h$$

$$\gamma = A_F/h^2, \quad \bar{E}_F = E_F/G_M, \quad \text{and} \quad \bar{E}_M = E_M/G_M. \tag{14}$$

Using equations (4) - (8) and equations (14), the equilibrium equations, equations (1), (2), and (3), may be written in terms of the displacements as

$$\bar{E}_F\gamma \frac{d^2}{d\eta^2}[U_{m,n}] + \frac{1}{2}\frac{d}{d\eta}[V_{m+1,n} - V_{m-1,n} + W_{m,n+1} - W_{m,n-1}] + U_{m+1,n} + U_{m-1,n} + U_{m,n+1} + U_{m,n-1} - 4U_{m,n} = 0 , \tag{15}$$

$$\bar{E}_M[V_{m+1,n} - 2V_{m,n} + V_{m-1,n}] + \frac{1}{2}\{\frac{1}{2}\frac{d^2}{d\eta^2}[V_{m+1,n} + 2V_{m,n} + V_{m-1,n}] + \frac{d}{d\eta}[U_{m+1,n} - U_{m-1,n}]\} = 0 , \text{ and} \tag{16}$$

$$\bar{E}_M[W_{m,n+1} - 2W_{m,n} + W_{m,n-1}] + \frac{1}{2}\{\frac{1}{2}\frac{d^2}{d\eta^2}[W_{m,n+1} + 2W_{m,n} + W_{m,n-1}] + \frac{d}{d\eta}[U_{m,n+1} - U_{m,n-1}]\} = 0. \tag{17}$$

It is now assumed that functions $\bar{U}(\eta, \theta, \phi)$, $\bar{V}(\eta, \theta, \phi)$, and $\bar{W}(\eta, \theta, \phi)$ exist such that the normalized displacements $U_{m,n}$, $V_{m,n}$, and $W_{m,n}$ are the Fourier coefficients in a double Fourier series expansion. Then,

$$\bar{U}(\eta, \theta, \phi) = \sum_{r=-\infty}^{\infty}\sum_{s=-\infty}^{\infty} U_{r,s}(\eta)e^{-ir\theta}e^{-is\phi}, \tag{18}$$

$$\bar{V}(\eta, \theta, \phi) = \sum_{r=-\infty}^{\infty}\sum_{s=-\infty}^{\infty} V_{r,s}(\eta)e^{-ir\theta}e^{-is\phi}, \text{ and} \tag{19}$$

$$\overline{W}(\eta, \theta, \phi) = \sum_{r=-\infty}^{\infty} \sum_{s=-\infty}^{\infty} W_{r,s}(\eta) e^{-ir\theta} e^{-is\phi} . \tag{20}$$

As the displacements are continuous functions of η, the representation given above is necessarily valid. These equations may be inverted to yield

$$U_{m,n}(\eta) = \frac{1}{4\pi^2} \int_{-\pi}^{\pi} \int_{-\pi}^{\pi} \overline{U}(\eta, \theta, \phi) e^{im\theta} e^{in\phi} \, d\theta d\phi, \tag{21}$$

$$V_{m,n}(\eta) = \frac{1}{4\pi^2} \int_{-\pi}^{\pi} \int_{-\pi}^{\pi} \overline{V}(\eta, \theta, \phi) e^{im\theta} e^{in\phi} \, d\theta d\phi, \text{ and} \tag{22}$$

$$W_{m,n}(\eta) = \frac{1}{4\pi^2} \int_{-\pi}^{\pi} \int_{-\pi}^{\pi} \overline{W}(\eta, \theta, \phi) e^{im\theta} e^{in\phi} \, d\theta d\phi. \tag{23}$$

The equilibrium equations may then be written in terms of the functions $\overline{U}$, $\overline{V}$, and $\overline{W}$ as

$$\overline{E}_F \gamma \frac{d^2\overline{U}}{d\eta^2} + i \sin(\theta) \frac{d\overline{V}}{d\eta} + i \sin(\phi) \frac{d\overline{W}}{d\eta} + 2\overline{U} [\cos(\theta) + \cos(\phi) - 2] = 0, \tag{24}$$

$$\frac{1}{2} [1 + \cos(\theta)] \frac{d^2\overline{V}}{d\eta^2} - 2\overline{E}_M [1 - \cos(\theta)] \overline{V} + i \sin(\theta) \frac{d\overline{U}}{d\eta} = 0, \text{ and} \tag{25}$$

$$\frac{1}{2} [1 + \cos(\phi)] \frac{d^2\overline{W}}{d\eta^2} - 2\overline{E}_M [1 - \cos(\phi)] \overline{W} + i \sin(\phi) \frac{d\overline{U}}{d\eta} = 0. \tag{26}$$

These three second order differential equations can be written as uncoupled sixth order equations and if the boundary condition of vanishing displacements for large η, equation (9), is enforced, the solutions then will have the following form.

$$\bar{U}\ (\eta,\ \theta,\ \phi) = A_1 e^{-D_1\eta} + A_2 e^{-D_2\eta} + A_3 e^{-D_3\eta} \tag{27}$$

$$\bar{V}\ (\eta,\ \theta,\ \phi) = B_1 e^{-D_1\eta} + B_2 e^{-D_2\eta} + B_3 e^{-D_3\eta} \tag{28}$$

$$\bar{W}\ (\eta,\ \theta,\ \phi) = C_1 e^{-D_1\eta} + C_2 e^{-D_2\eta} + C_3 e^{-D_3\eta} \tag{29}$$

where D_1, D_2, D_3 must have positive real parts. Substituting into equations (25) and (26) the relationships between B_k, C_k, and A_k, are determined as

$$B_k = \frac{i\ A_k D_k\ \sin\ (\theta)}{\frac{1}{2}\ [1 + \cos\ (\theta)]\ D_k^2 - 2\bar{E}_M\ [1 - \cos\ (\theta)]} \qquad \text{and} \tag{30}$$

$$C_k = \frac{i\ A_k D_k\ \sin\ (\phi)}{\frac{1}{2}\ [1 + \cos\ (\phi)]\ D_k^2 - 2\bar{E}_M\ [1 - \cos\ (\phi)]}\ , \tag{31}$$

where k = 1, 2, 3. Equation (24) then gives a sixth order algebraic equation for D_k of the form

$$\alpha_1 D_k^6 + \alpha_2 D_k^4 + \alpha_3 D_k^2 + \alpha_4 = 0\ . \tag{32}$$

The coefficients α_i are

$$\alpha_1 = \frac{\gamma \bar{E}_F}{4}[1 + \cos(\theta)][1 + \cos(\phi)], \tag{33}$$

$$\alpha_2 = -2\gamma \bar{E}_F \bar{E}_M [1 - \cos(\theta)\cos(\phi)], \tag{34}$$

$$\alpha_3 = 2\bar{E}_M \Big\{ [1 - \cos(\theta)]\{\gamma \bar{E}_F \bar{E}_M [1 - \cos(\phi)] + [1 + \cos(\phi)] \times [1 - \cos(\theta)]\} + [1 - \cos(\phi)]\{\gamma \bar{E}_F \bar{E}_M [1 - \cos(\theta)] + [1 + \cos(\theta)][1 - \cos(\phi)]\}\Big\}, \text{ and} \tag{35}$$

$$\alpha_4 = 8\bar{E}_M^2 [1 - \cos(\theta)][1 - \cos(\phi)][\cos(\theta) + \cos(\phi) - 2]. \tag{36}$$

Letting $D_k^2 = \xi_k$, the six roots can be obtained and, in order to satisfy equation (9), the three roots with position real parts are taken.

It is noted that all roots of equation (32) vanish at $\theta = \phi = 0$ and unbounded roots exist at $\theta = \phi = \pm\pi$. The first is clearly seen from the fact that if $\theta = \phi = 0$ then $\alpha_2 = \alpha_3 = \alpha_4 = 0$. For $\theta = \phi = \pm\pi$, $\alpha_1 = \alpha_2 = 0$ and the resulting equation gives

$$D_2 = +\sqrt{8/\gamma \bar{E}_F}, \qquad \theta = \phi = \pi. \tag{37}$$

It also follows that the remaining roots must be unbounded and therefore letting $\theta = \phi = \alpha \longrightarrow \pm\pi$, then

$$D_1 = D_3 = \sqrt{8\bar{E}_M/[1+\cos(\alpha)]}\ . \tag{38}$$

This is the same value as the one singular root found in the two-dimensional case [18]. An additional special case exist when either θ or ϕ equals zero as α_4 is then zero and therefore D_2 must vanish. The remaining two roots

are

$$D_1,\quad D_3 = \left\{\frac{2\bar{E}_M[\,1-\cos(\alpha)\,]}{[\,1+\cos(\alpha)\,]}\left[1 \pm \sqrt{1 - \frac{2[\,1+\cos(\alpha)\,]}{\gamma \bar{E}_F \bar{E}_M}}\right]\right\}^{1/2} \tag{39}$$

where if $\theta = 0$, $\alpha = \phi$ and for $\phi = 0$, $\alpha = \theta$. The positive sign is taken for D_1 and the negative sign for D_3.

The functions A_1, A_2, and A_3, which depend on θ and ϕ , are next determined from the boundary conditions, where equation (9) is satisfied by the proper choice of D_1, D_2, D_3. Equation (10) gives

$$\frac{1}{4\pi^2}\int_{-\pi}^{\pi}\int_{-\pi}^{\pi}[A_1 + A_2 + A_3]e^{im\theta}e^{in\phi}d\theta d\phi = 0 \tag{40}$$

for all unbroken fibers, and equation (11) gives

$$\frac{1}{4\pi^2}\int_{-\pi}^{\pi}\int_{-\pi}^{\pi}[A_1D_1 + A_2D_2 + A_3D_3]e^{im\theta}e^{in\phi}d\theta d\phi = 1 \tag{41}$$

for all broken fibers.

The conditions of vanishing shear stresses on $\eta = 0$ specified by equations (12) and (13) require the following relations between the three functions A_1, A_2, A_3:

$$A_2 = -A_1\frac{D_1^2 - D_3^2}{D_2^2 - D_3^2} \tag{42}$$

$$\times\ \frac{\{[\,1+\cos(\phi)\,]D_2^2 - 4\bar{E}_M[\,1-\cos(\phi)\,]\}\{[\,1+\cos(\theta)\,]D_2^2 - 4\bar{E}_M[\,1-\cos(\theta)\,]\}}{\{[\,1+\cos(\phi)\,]D_1^2 - 4\bar{E}_M[\,1-\cos(\phi)\,]\}\{[\,1+\cos(\theta)\,]D_1^2 - 4\bar{E}_M[\,1-\cos(\theta)\,]\}},$$

and

$$A_3 = -A_1\frac{D_1^2 - D_2^2}{D_3^2 - D_2^2} \tag{43}$$

$$\times\ \frac{\{[\,1+\cos(\phi)\,]D_3^2 - 4\bar{E}_M[\,1-\cos(\phi)\,]\}\{[\,1+\cos(\theta)\,]D_3^2 - 4\bar{E}_M[\,1-\cos(\theta)\,]\}}{\{[\,1+\cos(\phi)\,]D_1^2 - 4\bar{E}_M[\,1-\cos(\phi)\,]\}\{[\,1+\cos(\theta)\,]D_1^2 - 4\bar{E}_M[\,1-\cos(\theta)\,]\}}$$

Equations (40) and (41) then reduce to a set of dual integral equations in terms of the unknown function $A_1(\theta,\phi)$. Proceeding in the same manner as [18], based on the orthogonality of the Fourier series, these dual integral equations can be reduced to a set of simultaneous linear algebraic equations. Equation (40) is identically satisfied by assuming

$$\frac{1}{4\pi^2}\,[A_1 + A_2 + A_3] = \sum_r \sum_s H_{r\,s} e^{-ir\theta}\, e^{-is\phi} \tag{44}$$

where r and s correspond to the indices of the broken fibers and the $H_{r,s}$ are constants. Substituting from equations (42) and (43) into equations (40), (41), and (44) then reduces equation (41) to a set of algebraic equations for the $H_{r,s}$. The set of equations are developed as follows. Referring to equations (42) and (43), let

$$A_2 = \beta_2 A_1, \text{ and} \tag{45}$$

$$A_3 = \beta_3 A_1. \tag{46}$$

Then, from equation (44)

$$\frac{1}{4\pi^2}\,[1 + \beta_2 + \beta_3]A_1 = \sum_r \sum_s H_{r,s} e^{-ir\theta}\, e^{-is\phi} \tag{47}$$

and equation (41) is then

$$\sum_r \sum_s H_{r,s} \int_{-\pi}^{\pi} \int_{-\pi}^{\pi} \frac{D_1 + \beta_2 D_2 + \beta_3 D_3}{1 + \beta_2 + \beta_3}\, e^{-ir\theta}\, e^{-is\phi}\, e^{im\theta}\, e^{in\phi}\, d\theta d\phi = 1, \tag{48}$$

where m, n, r, s correspond to broken fibers. With the constants $H_{r,s}$ then known, the A_k, B_k, and C_k are specified and the stresses and displacement can be calculated.

In the numerical evaluation of equation (48) as well as the stress and

displacement equations, the singular behaviour of D_1 and D_3 at $\theta = \phi = +\pi$ and the behaviour of D_1, D_2, and D_3 along the lines θ or $\phi = 0$ or π, must be accounted for. Noting the form of β_2 and β_3 given by equations (40), (41), (43), and (44) and the fact that $D_1 = D_3 = \sqrt{8\bar{E}_M/[1+\cos(\alpha)]}$ as $\theta = \phi = \alpha \to \pm\pi$, it is seen that $\beta_2 = \beta_3$ in the limit. Proceeding to the limit as $\alpha \to \pm\pi$, the integrand of equation (48) then remains bounded and equals D_1 at $\theta = \phi = \pi$. The analogous behavior occurs in the two-dimensional case [18]. For either θ or ϕ equal to zero the integrand of equation (48) is bounded and vanishes at $\theta = \phi = 0$. In a similar manner all stress and displacement equations have bounded integrands at all points in the region of integration.

SYMMETRIC ARRAY OF BROKEN FIBERS

The above equations can be simplified considerably for the special case of a symmetric array of broken fibers. For convenience in comparing the two solutions only those equations which change due to the symmetry restriction will be recorded and they will be indicated by the previous equation number with an asterisk.

If a symmetric number of fibers is assumed to be broken with respect to the y and z axes it then follows that the displacement $U_{m,n}(\eta)$ is even valued on the indices m and n, while the displacement $V_{m,n}(\eta)$ is odd valued on m and even valued on n, and the displacement $W_{m,n}(\eta)$ is even valued on m and odd valued on n. Equations (18) - (26) then become:

$$\overline{U}(\eta, \theta, \phi) = \sum_{r=o}^{\infty}{}' \sum_{s=o}^{\infty}{}' U_{r,s}(\eta) \cos(r\theta) \cos(s\phi), \tag{18}*$$

$$\overline{V}(\eta, \theta, \phi) = \sum_{r=1}^{\infty} \sum_{s=o}^{\infty}{}' V_{r,s}(\eta) \sin(r\theta) \cos(s\phi), \tag{19}*$$

$$\overline{W}(\eta, \theta, \phi) = \sum_{r=o}^{\infty}{}' \sum_{s=1}^{\infty} W_{r,s}(\eta) \cos(r\theta) \sin(s\phi), \tag{20}*$$

$$U_{m,n}(\eta) = \frac{4}{\pi^2} \int_o^{\pi} \int_o^{\pi} \overline{U}(\eta, \theta, \phi) \cos(m\theta) \cos(n\phi)\, d\theta d\phi, \tag{21}*$$

$$V_{m,n}(\eta) = \frac{4}{\pi^2} \int_o^{\pi} \int_o^{\pi} \overline{V}(\eta, \theta, \phi) \sin(m\theta) \cos(n\phi)\, d\theta d\phi, \tag{22}*$$

$$W_{m,n}(\eta) = \frac{4}{\pi^2} \int_o^{\pi} \int_o^{\pi} \overline{W}(\eta, \theta, \phi) \cos(m\theta) \sin(n\phi)\, d\theta d\phi, \tag{23}*$$

$$\gamma \overline{E}_F \frac{d^2\overline{U}}{d\eta^2} + \sin(\theta) \frac{d\overline{V}}{d\eta} + \sin(\phi) \frac{d\overline{W}}{d\eta} + 2\overline{V} [\cos(\theta) + \cos(\phi) - 2] = 0, \tag{24}*$$

$$\frac{1}{2}[1 + \cos(\theta)]\frac{d^2\overline{V}}{d\eta^2} - 2\overline{E}_m[1 - \cos(\theta)]\overline{V} - \sin(\theta)\frac{d\overline{U}}{d\eta} = 0, \qquad (25)^*$$

$$\frac{1}{2}[1 + \cos(\phi)]\frac{d^2\overline{W}}{d\eta^2} - 2\overline{E}_M[1 - \cos(\phi)]\overline{W} - \sin(\phi)\frac{d\overline{U}}{d\eta} = 0. \qquad (26)^*$$

Equations (27), (28), and (29) remain unchanged, and equations (30) and (31) become

$$B_k = \frac{-A_K D_K \sin(\theta)}{\frac{1}{2}[1 + \cos(\theta)]D_K^2 - 2\overline{E_M}[1 - \cos(\theta)]}, \text{ and} \qquad (30)^*$$

$$C_K = \frac{-A_K D_K \sin(\phi)}{\frac{1}{2}[1 + \cos(\phi)]D_K^2 - 2\overline{E_M}[1 - \cos(\phi)]} \qquad (31)^*$$

The coefficients α_1, α_2, α_3, and α_4 are unchanged as are the roots to the characteristic equation (32). The remaining changes are in equations (40), (41), (44), (47), and (48) as

$$\frac{4}{\pi^2}\int_0^{\pi}\int_0^{\pi}[A_1 + A_2 + A_3]\cos(m\theta)\cos(n\phi)\,d\theta d\phi = 0, \qquad (40)^*$$

$$\frac{4}{\pi^2}\int_0^{\pi}\int_0^{\pi}[A_1D_1 + A_2D_2 + A_3D_3]\cos(m\theta)\cos(n\phi)\,d\theta d\phi = 1, \qquad (41)^*$$

$$\frac{4}{\pi^2}[A_1 + A_2 + A_3] = \sum_r\sum_s H_{r,s}\cos(r\theta)\cos(s\phi), \qquad (44)^*$$

$$\frac{4}{\pi^2}[1 + \beta_2 + \beta_3]A_1 = \sum_r\sum_s H_{r,s}\cos(r\theta)\cos(s\phi). \text{ and} \qquad (47)^*$$

$$\sum_r \sum_s H_{r,s} \int_0^{\pi} \int_0^{\pi} \frac{D_1+\beta_2 D_2+\beta_3 D_3}{1+\beta_2+\beta_3} \cos(r\theta)\cos(s\phi)\cos(m\theta)\cos(n\phi)\, d\theta d\phi = 1. \quad (48)*$$

NUMERICAL SOLUTION AND RESULTS

A computer code has been developed for the numerical solution of the above equations. The program was written in FORTRAN IV language for the NASA-Langley Research Center CDC computer.[1] A maximum error of less than 1 percent was achieved with the average computation time being on the order of thirty minutes.

The results presented below concern comparisons between the present three-dimensional solution, the two-dimensional studies of [16] and [18], and the three-dimensional shear-lag problem of [17]. Differences in the respective two- and three-dimensional analyses due to the inclusion of the matrix normal stresses in the model are central in the discussion. Detailed results are given apropos the manner of distribution of critical matrix normal and shear stresses, and the rate of decay of fiber stress as a function of distance from broken fibers. All results are for $\bar{E}_M = 2.0$, $\bar{E}_F = 5.2$. Changes in material properties do not change the form of the solution and it was felt to be more important to discuss the fundamental differences in the various solutions and to investigate the significance of the geometric parameters, i.e. fiber spacing and number of broken fibers.

It is important to note that in ([18], equation (2.1)), the equilibrium equation in the transverse direction, was written as

$$\sigma_n - \sigma_{n-1} + \frac{b}{2}\frac{d}{dy}(\tau_n + \tau_{n-1}) = 0.$$

---

[1] The program is entitled, "Stresses in a Three-Dimensional Unidirectional Composite Containing Broken Fibers," and is available through COSMIC, 112 Barrow Hall, The University of Georgia, Athens, GA 30602.

This amounts to assuming that the fiber supports all of the shear stress. We have changed this equation by replacing b with h to be consistent with the present analysis. The results for the two-dimensional geometry presented in this paper were obtained by solving the appropriately modified equations of [18]. These changes gave insignificant differences in the fiber stress but resulted in considerable changes in the matrix stresses.

The constants γ and h deserve further discussion as changes in parameters can be interpreted to imply significantly different physical situations. That is, if δ is taken as the distance between fiber boundaries, the relationship between γ, h, and δ and the approximations assumed for the matrix surface over which stresses are transferred and strains calculated are open to considerable freedom of definition, while still remaining within the validity of the formulation for both the two- and three-dimensional models. The geometry of Figure 2 and the corresponding geometry of [16], [17], and [18] requires only that the distance h be consistent in all three equilibrium equations.

For example, referring to Figures 2 and 3 and to equations (1) through (8), it is seen that h is the width in the vertical plane over which the shear stresses act in equation (1), while in equations (2) and (3), it is the corresponding distance in the horizontal plane. In equations (5) through (8), it is related to the distance through which the matrix deformations take place, and should be bounded by the distance between fiber centers, $b + \delta$, and the minimum spacing between fibers, δ. As seen below, the width in equation (1) need not be the same as the distance in equations (2) and (3) or (5) through (8).

In Figures 6 and 7 three different geometries and corresponding assumptions γ, h, and δ are given for the two- and three-dimensional models, respectively. The different value of γ for each case is due to the particular geometry assumed and is derived by writing the equilibrium equation in the axial direction, accounting for the specific fiber shape and shear transfer region. Table 1 gives values of γ for particular values of δ for each case of Figures 6 and 7.

Case I in Figures 6 and 7 corresponds to assuming that the fibers have the same material properties in shear and transverse normal directions as the matrix, and would be more appropriate for nearly equal fiber-matrix properties.

Cases II and III are more realistic for a typical composite, in which the fibers usually have a much higher modulus than the matrix, and make the assumption that the normal and shear strains occur over a critical distance equal to the minimum distance between fibers. The main difference between II and III is the assumed shape of the fiber. The decision as to whether a square or circular fiber cross-section is more appropriate is based on considering the solutions for close fiber spacing and comparing the manner in which the stresses increase with decreasing δ with previous elasticity solutions [19] and [20]. In these studies the stresses between two circular cylinders under the action of inplane loading and transverse shear, respectively, were considered. In both studies the numerical results indicated a $1/\sqrt{\delta}$ behavior for the maximum stresses between rigid cylinders as the distance δ approached zero. For elastic cylinders unbounded stresses did not occur. Cases II and III are equivalent to assuming infinite transverse normal and shear material properties for the fibers as all the strain is assumed to occur over the distance between fibers; therefore, it seems consistent to seek a model having matrix stresses which behave as $1/\sqrt{\delta}$

if possible. From Figures 6 and 7, Cases II and III, the matrix material supporting the stresses decreases like $1/h$ and $1/h^2$, respectively, and the stresses should increase more repidly with decreasing h in III than II. By considering the present solution along with [16], [17], and [18] and expanding the equations for small values of h, where $h = \delta$, the matrix stresses for all four models are found to increase as $0(1/\sqrt{h})$ and $0(1/h)$ for Cases II and III, respectively.

Case II is then more appropriate for close fiber spacing as it agrees with the continuum solutions [19] and [20], and it is suggested that the actual fiber cross-section be represented as an "equivalent" square cross-section having equal areas. All results given below are for Case II with the corresponding γ, h, and δ relationship of Figures 6 and 7 and Table 1.

Figure 8 gives the value of the maximum stresses as a function of h for a square array of twenty five broken fibers, (five broken fibers in the two-dimensional study [18]). The stresses for [18] are larger for all values of spacing h due to the added constraint of the present geometry. As the number of broken fibers increase, the two solutions should approach each other. This is indicated in Table 2 for the particular case of one by eleven broken fibers i.e. (0,-5) through (0,5) where the stresses adjacent to the (1,0) fiber are compared with the stresses adjacent to the first unbroken fiber for one broken fiber in [18].

Both the normal and shear stresses are of considerable importance in formulating a failure criterion capable of predicting matrix damage. It is seen in Figures 9 and 10 that compressive normal stresses exist over part of the matrix region between the last broken and the first unbroken fiber, both in [18] and the present study. The shear stresses decrease due to the different boundary conditions at $\eta = 0$, from the corresponding shear-lag stresses;

therefore, it seems likely that the shear-lag model would lead to a prediction of greater matrix damage parallel to the fibers than the present model. Indeed, related two-dimensional shear-lag studies concerning matrix splitting for a unidirectional laminate (see [21] for one broken fiber and [22] for an arbitrary number of broken fibers with splitting and yielding) indicate that only a very small increase in the stress required to initiate damage can be tolerated before unstable splitting occurs. The splitting develops in the region adjacent to the last broken fiber which, as mentioned above, also has compressive stresses using the model of [18] without damage. The analysis of [22] is being extended to include a model having normal stresses in the matrix, and it is hoped that the results will be more consistent with experimental evidence, in which case local, stable, splitting has been observed [23] and [24]. Such behavior has also been observed at the NASA-Langley Research Center for Boron/Aluminum composites by C. C. Poe, (private communication).

An equally interesting observation is noted for the region between the first and second unbroken fibers. As indicated in Figures 9 and 10, the shear stress is considerably reduced from its value on the opposite side of the fiber; however, it is larger than the corresponding shear-lag solution. More importantly, it is opposite sign than the shear-lag stress. The normal stress is tensile and more than fifty percent larger than the maximum shear stress in the adjacent region. First-ply matrix splitting has been noted for bonded joints [25] which are very similar geometrically to the region in the vicinity of the notch in the present work and the large tensile stress found here certainly admits the possibility of such damage.

Table 3 gives results using the present solution for a square array of broken fibers as well as analogous results from [16], [17], and [18]. The maximum fiber stress occurs on the plane of the break ($\eta = 0$) and in the first

unbroken fiber at the center of the sides for the three-dimensional problems and in the first unbroken fiber in the two-dimensional problems. For both the two- and three-dimensional solutions, the maximum fiber stress is seen to be slightly smaller for the shear-lag model. Both the fiber and matrix stresses are larger in the two-dimensional case [18] than the present solution.

Figure 11 gives the magnitude of the maximum fiber stress in the first unbroken fiber as a function of the number of broken fibers for a square array, and compares these values with [16], [17], and [18]. Also, for the one particular case of eighty-one (nine) broken fibers, the stress in the first four unbroken fibers is given. The decrease in stress is largest between the first and second intact fibers with the rate of change being relatively small from that point on. As seen in the figure, the influence of the broken fibers decreases more slowly for the two-dimensional model [18] than for the present three-dimensional model.

CONCLUSIONS

The significant difference between the present model (either two- or three-dimensional) and the corresponding shear-lag model is in the change in the manner of distribution of the critical shear stress in the matrix and the introduction of matrix normal stresses. As noted, the critical shear stresses are reduced on the order of fifty percent over the corresponding shear-lag solution and the matrix normal stresses are found to be of sufficient magnitude to suggest potential matrix damage. For close fiber spacing both the normal and shear stresses in the matrix are shown to increase without bound and an equivalent cross-section is proposed which gives the correct singular behavior based on previously published elasticity solutions.

Surprisingly, with these major changes in matrix stresses, the fiber stresses are relatively unchanged, i.e., approximately three percent higher than the corresponding shear-lag solution. The fiber stress in all solutions is essentially independent of fiber spacing.

It then seems reasonable to expect that any attempt to develop an analysis for the investigation of matrix damage must be based on a more complete model than the shear-lag assumption.

REFERENCES

1. Verette, R. M. and Labor, J. D., "Structural Criteria for Advanced Composites," Northrop Corporation, USAF Contract F33615-74-C-5182, Final Report, TR-AFFDL-TR-76-142, March 1977.

2. Goree, J. G., "Crack Growth in Bonded Isotropic and Orthotropic Elastic Half-Planes," Annual Report NASA Grant NSG-1297, October 1977.

3. Poe, C. C. Jr., "Stress-Intensity Factor for a Cracked Sheet with Riveted and Uniformly Spaced Stringers," NASA TR R-358, 1971.

4. Swift, T., "Fracture Analysis of Adhesively Bonded Cracked Panels," J. Engr. Mat. and Tech., Vol. 100, (Jan. 1978), pp. 10-15.

5. Ratwani, M. M., "A Parametric Study of Fatigue Crack Growth Behavior in Adhesively Bonded Metallic Structures," J. Engr. Mat. and Tech., Vol. 100, (Jan. 1978), pp. 46-51.

6. Cook, T. S. and Erdogan, F., "Stresses in Bonded Materials with a Crack Perpendicular to the Interface," Int. J. Engr. Science, Vol. 10, (Nov. 1972), pp. 677-697.

7. Erdogan, F. and Biricikoglu, V., "Two Bonded Half-Planes with a Crack Going through the Interface," NASA-TR-72-4, June 1974.

8. Dalade, F. and Erdogan, F., "Fracture of Composite Orthotropic Plates Containing Periodic Buffer Strips," Lehigh University Research Report, NASA Grant NGR39-007-011, 1976.

9. Goree, J. G. and Venezia, W. A., "Bonded Elastic Half-Planes with an Interface Crack and a Perpendicular Intersecting Crack that Extends into the Adjacent Material - Part II," Int. J. Engr. Science, Vol. 1, (Jan. 1977), pp. 1-17

10. Goree, J. G. and Venezia, W. A., "Bonded Elastic Half-Planes with an Interface Crack and a Perpendicular Intersecting Crack that Extends into the Adjacent Material - Part II," Int. J. Engr. Science, Vol. 1, (Jan. 1977), pp. 19-27.

11. Gecit, M. R., and Erdogan, F., "The Effect of Adhesive Layers on the Fracture of Laminated Structures," J. Engr. Mat. and Tech., Vol. 100, (Jan. 1978), pp. 2-9.

12. Pagano, N. J. and Pipes, R. B., "Some Observations on the Interlaminar Strength of Composite Laminates," Int. J. Mech. Sci., Vol. 15, (1973), pp. 679.

13. Pagano, N. J., "On the Calculation of Interlaminar Normal Stress in Composite Laminates," J. Comp. Mat., Vol. 8, (1974), pp. 65.

14. Zweben, C., "Fracture Mechanics and Composite Materials: A Critical Analysis," Special Tech. Pub. 521, A.S.T.M., (1973), pp. 63-97.

15. Zweben, C., "An Approximate Method of Analysis for Notched Unidirectional Composites," Engr. Fracture Mech. Vol. 6, (1974), pp. 1-10.

16. Hedgepeth, J. M., "Stress Concentrations in Filamentary Structures," NASA TN D-882, May 1961.

17. Hedgepeth, J. M. and Van Dyke, P., "Local Stress Concentrations in Imperfect Filamentary Composite Materials," J. Comp. Mat., Vol. 1, (1967), pp. 294-309.

18. Eringen, A. C. and Kim, B. S., "Stress Concentrations in Filamentary Composites with Broken Fibers," Princeton University Tech. Report No. 36, (September 1973), ONR Contract N-00014-67-A-0151-0004.

19. Goree, J. G., "In-Plane Loading in an Elastic Matrix Containing Two Cylindrical Inclusions," J. Comp. Mat., Vol. 1, (1967), pp. 404-412.

20. Goree, J. G. and Wilson, H. B. Jr., "Transverse Shear Loading in an Elastic Matrix Containing Two Elastic Circular Cylindrical Inclusions," J. Appl. Mech., Vol. 34, (1967), pp. 511.

21. Hedgepeth, J. M. and Van Dyke, P., "Stress Concentrations from Single-Filament Failures in Composite Materials," Textile Res. Vol. 39, (1969), pp. 618-626.

22. Goree, J. G. and Gross, R. S., "Stresses in a Two-Dimensional Unidirectional Composite with Broken Fibers and Longitudinal Matrix Damage," Presented at the 15th Annual Meeting of the Society of Engineering Science, Gainesville, Florida, December 4-5, 1978.

23. Awerbuch, J. and Hahn, H. T., "Fracture Behavior of Metal Matrix Composites," Proc. of the Soc. of Engr. Sci., Recent Advances in Engr. Sci., (1977), pp. 343-350.

24. Waszczak, J. P., "On the Applicability of Linear Elastic Fracture Mechanics to 5.6-MIL Boron/6061 Aluminum," AIAA/ASME/SAE 16th Structures, Structural Dynamics, and Materials Conference, (1975), AIAA Paper No. 75-786.

25. Hart-Smith, L. J., "Adhesive-Bonded Double-Lap Joints," NASA CR-112235, January, 1973.

δ/b	2.00	1.50	1.25	1.00	0.75	0.50	0.25	0.10
γ_{I}^{1}	0.33	0.40	0.44	0.50	0.57	0.67	0.80	0.91
γ_{II}^{1}	0.50	0.67	0.80	1.00	1.33	2.00	4.00	10.00
γ_{III}^{1}	0.20	0.35	0. 50	0.79	1.40	3.14	12.57	78.57
γ_{I}^{2}	0.11	0.16	0.20	0.25	0.33	0.44	0.64	0.83
γ_{II}^{2}	0.50	0.67	0.80	1.00	1.33	2.00	4.00	10.00
γ_{III}^{2}	0.20	0.35	0.50	0.79	1.40	3.14	12.57	78.57

[1]Two-dimensional geometry, Figure 6.

[2]Three-dimensional geometry, Figure 7.

TABLE I. Relationship between the fiber spacing δ and the constant γ for the geometry of Figures 6 and 7.

Model	(3-D)[1]	(2-D)[2]	(3-D)[3]	(2-D)[4]
$\bar{\sigma}_x$	1.371	1.372	1.327	1.333
$\bar{\sigma}_y$	0.316	0.316	-	-
$\bar{\tau}_{xy}$	-0.238	-0.238	-0.343	-0.344

[1] present solution, fiber (1,0).

[2] two-dimensional solution [18], fiber (1).

[3] three-dimensional shear-lag [17], fiber (1,0).

[4] two-dimensional shear-lag [16], fiber (1).

TABLE 2. Comparison of maximum stresses for an array of one by eleven broken fibers in the three-dimensional model and one broken fiber in the two-dimensional case. The geometry of Figures 6 and 7 case II with $h = \delta = 1.0$, $\gamma = 1.0$ is used.

M[1]	$\bar{\sigma}_x$ (3-D)[2]	$\bar{\sigma}_x$ (2-D)[3]	$\bar{\sigma}_x$ (3-D)[4]	$\bar{\sigma}_x$ (2-D)[4]
1	1.171	1.384	1.146	1.333
9	1.521	1.908	1.456	1.828
25	1.821	2.318	1.728	2.216
49	2.087	2.666	1.967	2.546
81	2.321	2.974	2.181	2.838

[1] M equals the total number of broken fibers in the three-dimensional case. ($\sqrt{M}$ for the two-dimensional case)

[2] present solution.

[3] two-dimensional solution [18].

[4] shear-lag solutions [16], [17].

TABLE 3. Maximum fiber stress (stress concentration factor) for a square array of broken fibers, $h = \delta = 2.0$, $\gamma = 0.5$.

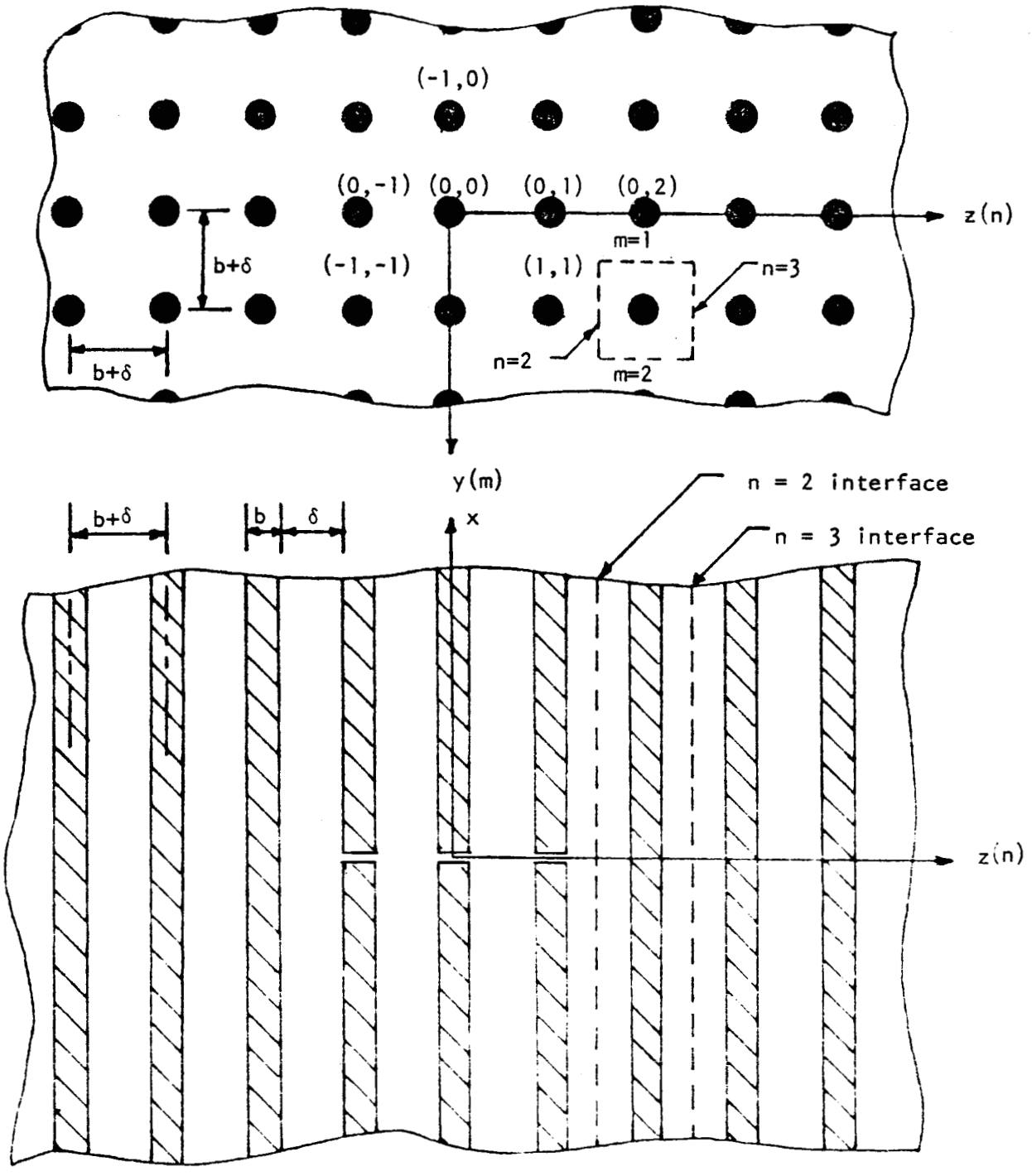

FIGURE 1. Three-dimensional array of parallel fibers.

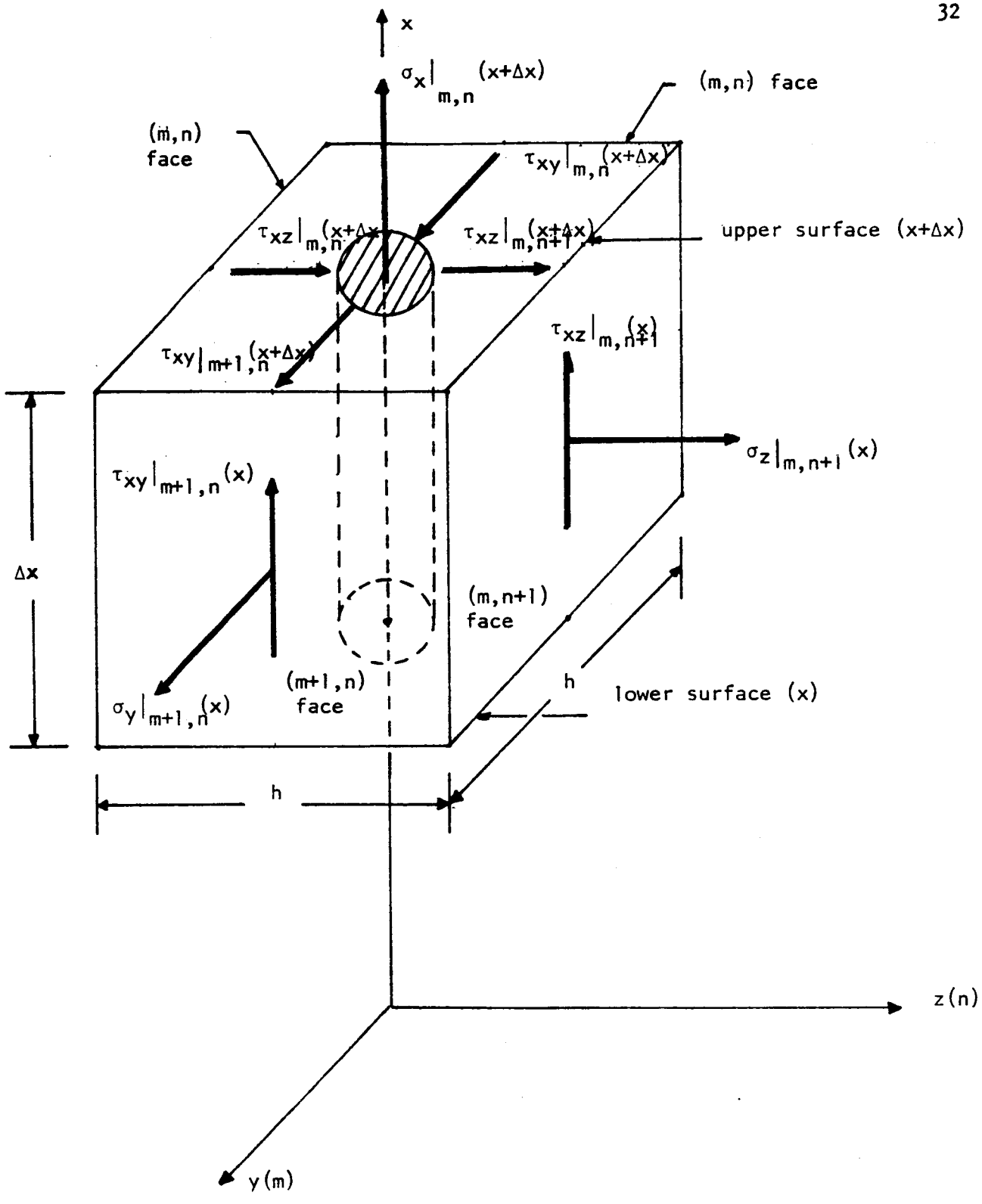

Figure 2. Free-body diagram for a typical element of the (m,n) fiber.

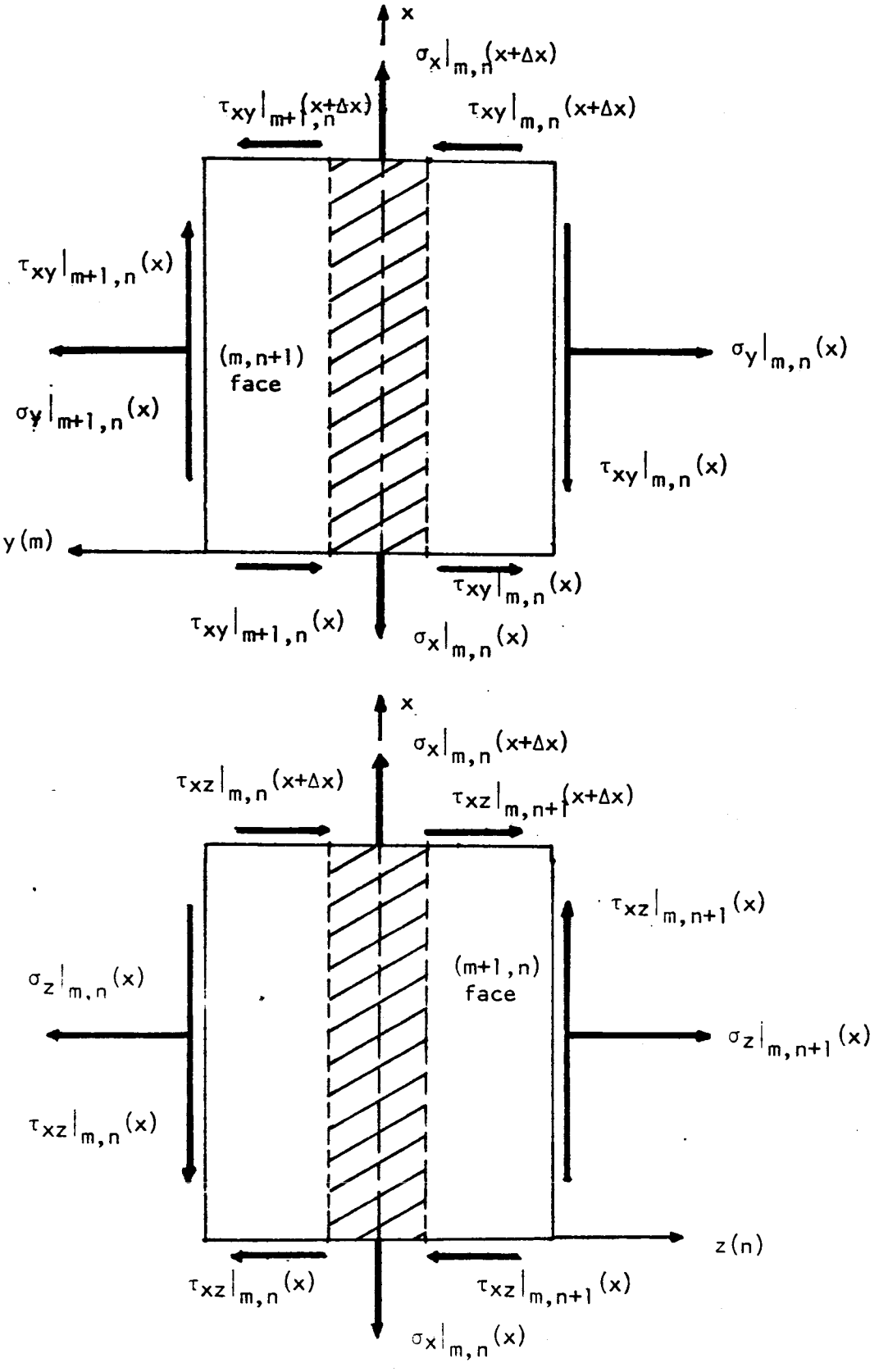

Figure 3. Side views of the free-body diagram of Figure 2.

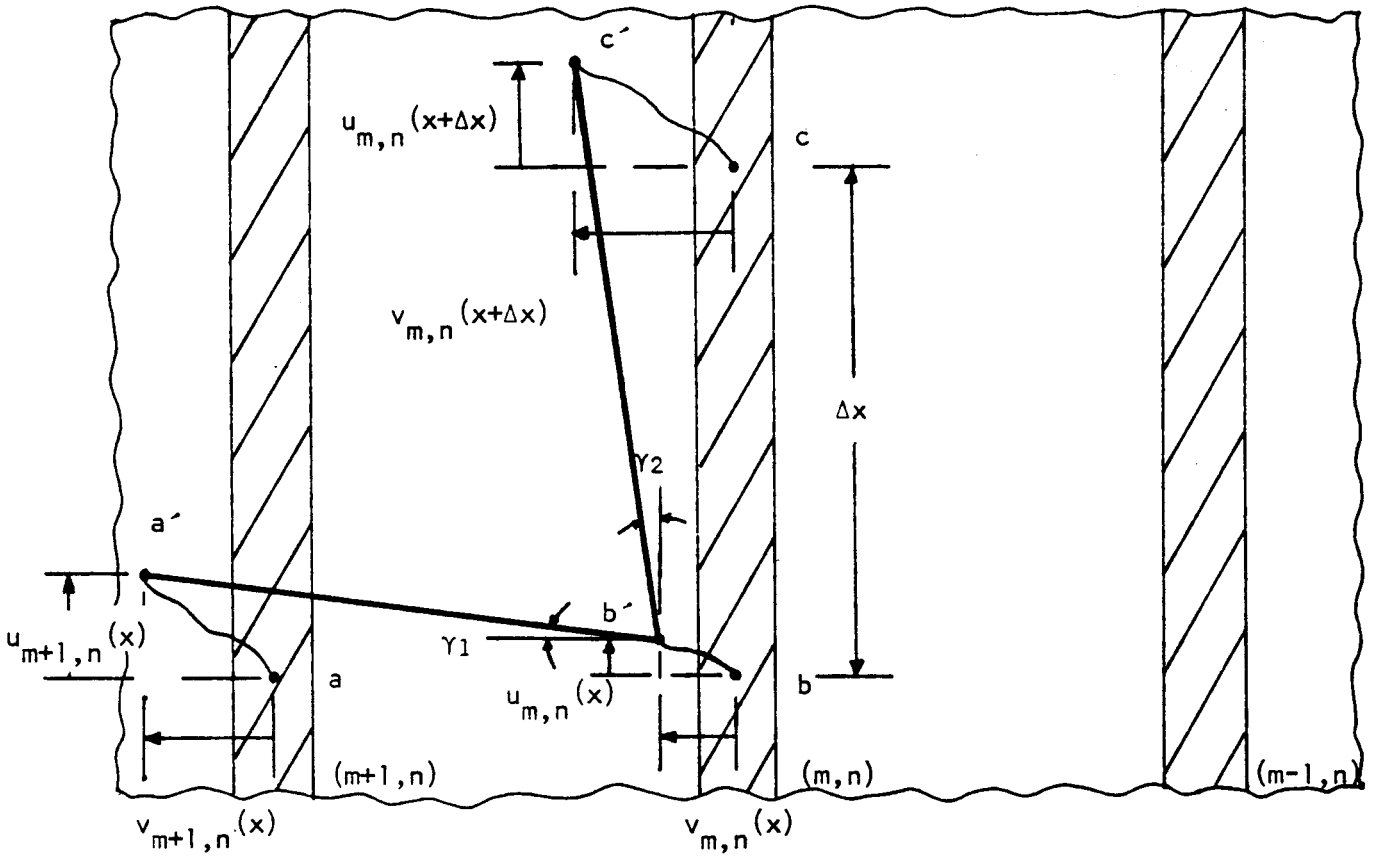

Plane "n" where (a, b, c) and (a´, b´, c´) are the points before and after deformation.

Note: To insure symmetry $\gamma_2 = \frac{1}{2}\frac{d}{dx}[v_{m+1,n} + v_{m,n}]$ rather than $\frac{d}{dx} v_{m,n}$.

Figure 4. Displacements for a region containing the m,n fiber. (x,y plane)

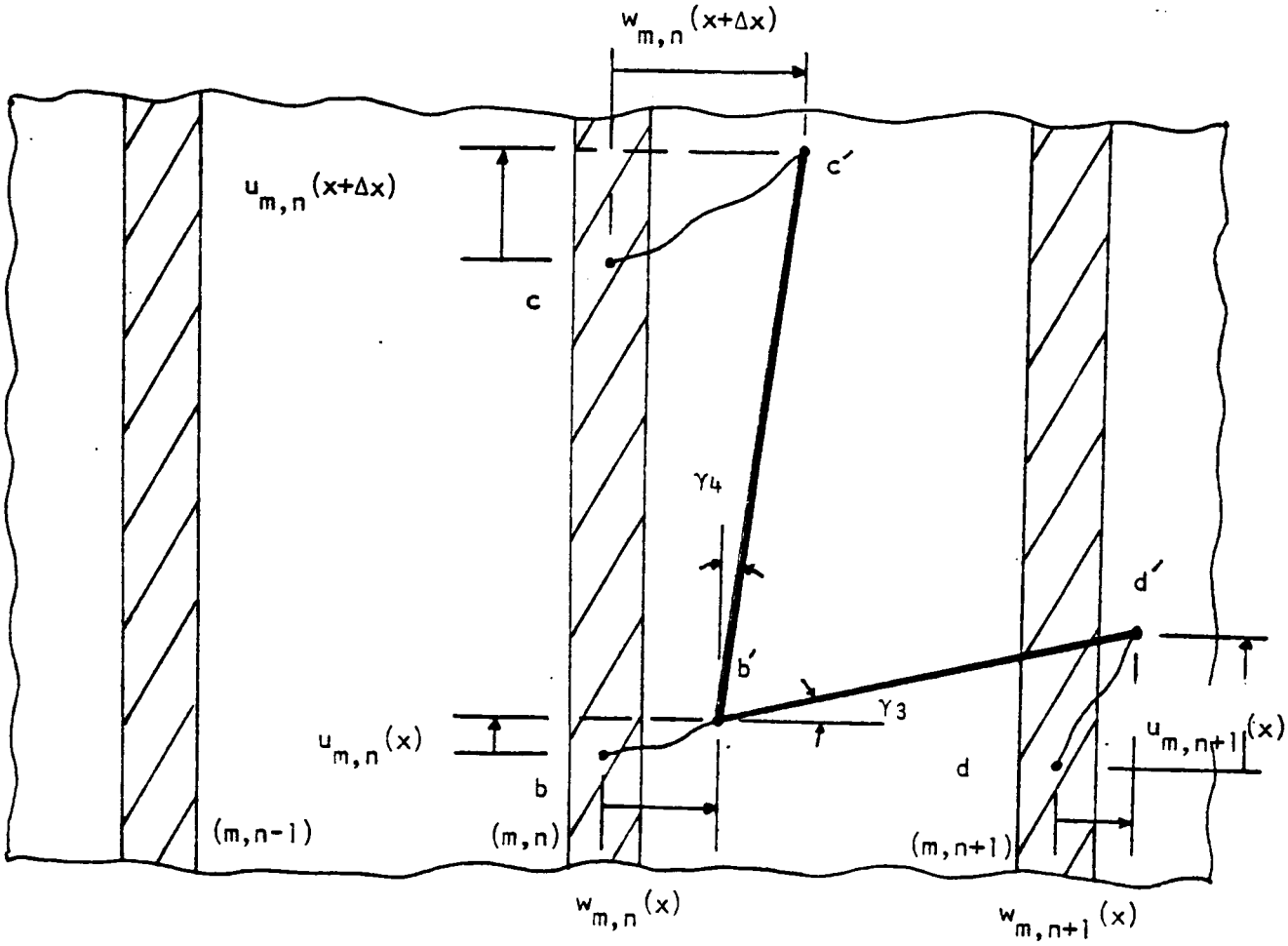

Plane "m" where (b, c, d) and (b′, c′, d′) are three points before and after deformation.

Note: To insure symmetry $\gamma_4 = \frac{1}{2}\frac{d}{dx}[w_{m,n+1} + w_{m,n}]$ rather than $\frac{d}{dx} w_{m,n}$.

Figure 5. Displacements for a region containing the m,n fiber. (x,z plane)

Case I

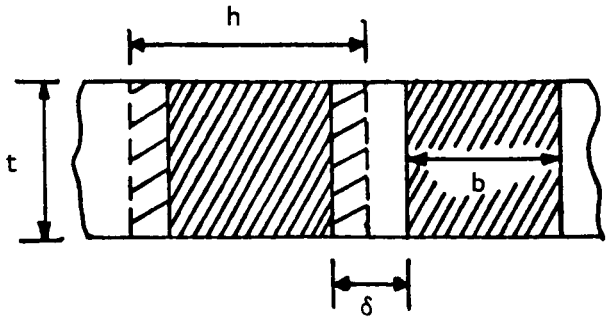

$\gamma_I = A_F/th = b/h$

$h = b + \delta, \quad h \geq b$

$V_F = b/h$

matrix stresses are $O(1)$ as $\delta \to 0$

Case II

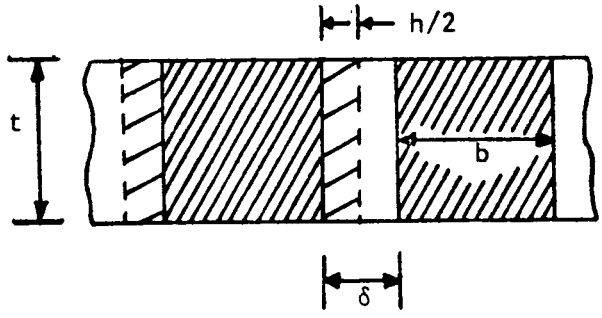

$\gamma_{II} = A_F/th = b/h$

$h = \delta, \quad h \geq 0$

$V_F = b/(b+\delta)$

matrix stresses are $O(1/\sqrt{\delta})$ as $\delta \to 0$

Case III

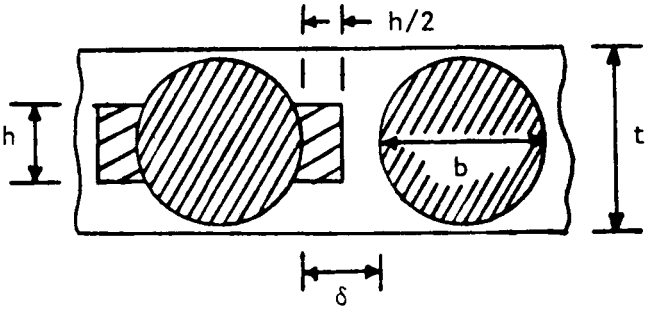

$\gamma_{III} = A_F/h^2$

$h = \delta, \; h \geq 0$

$V_F = A_F/(b+\delta)t$

matrix stresses are $O(1/\delta)$ as $\delta \to 0$

FIGURE 6. Geometry for the fiber-matrix cross-section, two-dimensional model.

Case I

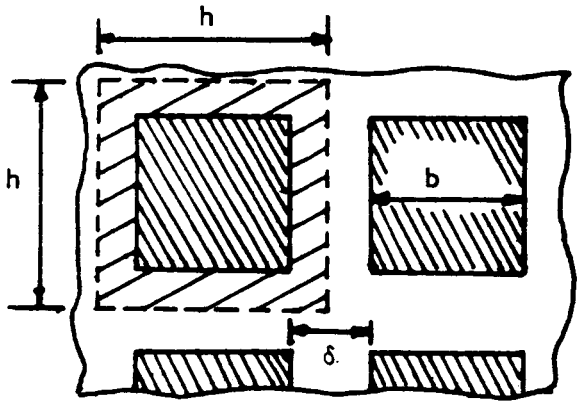

$\gamma_I = A_F/h^2 = b^2/h^2$

$h = b + \delta, \quad h \geq b$

$V_F = b^2/h^2$

matrix stresses are $O(1)$ as $\delta \to 0$

Case II

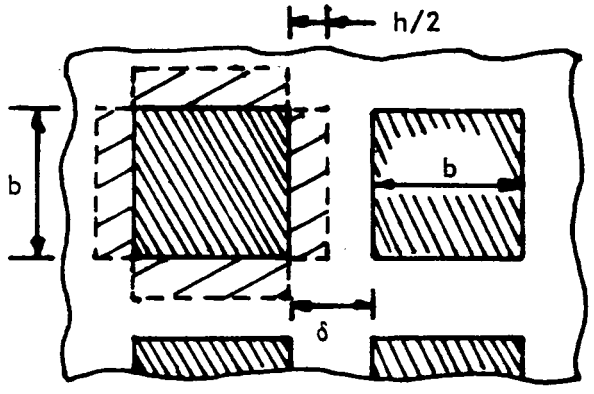

$\gamma_{II} = A_F/bh = b/h$

$h = \delta, \quad h \geq 0$

$V_F = b^2/(b+\delta)^2$

matrix stresses are $O(1/\sqrt{\delta})$ as $\delta \to 0$

Case III

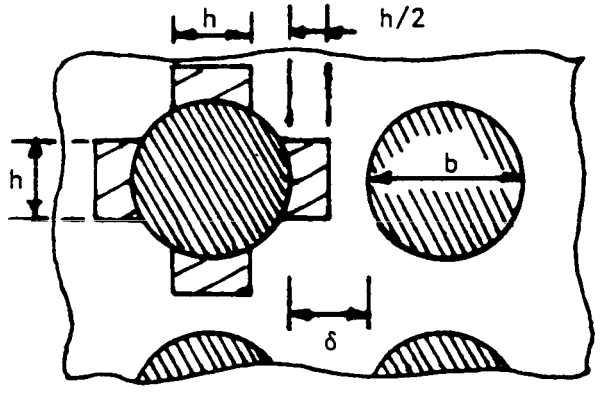

$\gamma_{III} = A_F/h^2$

$h = \delta, \quad h \geq 0$

$V_F = A_F/(b+\delta)^2$

matrix stresses are $O(1/\delta)$ as $\delta \to 0$

FIGURE 7. Geometry for the fiber-matrix cross-section, three-dimensional model.

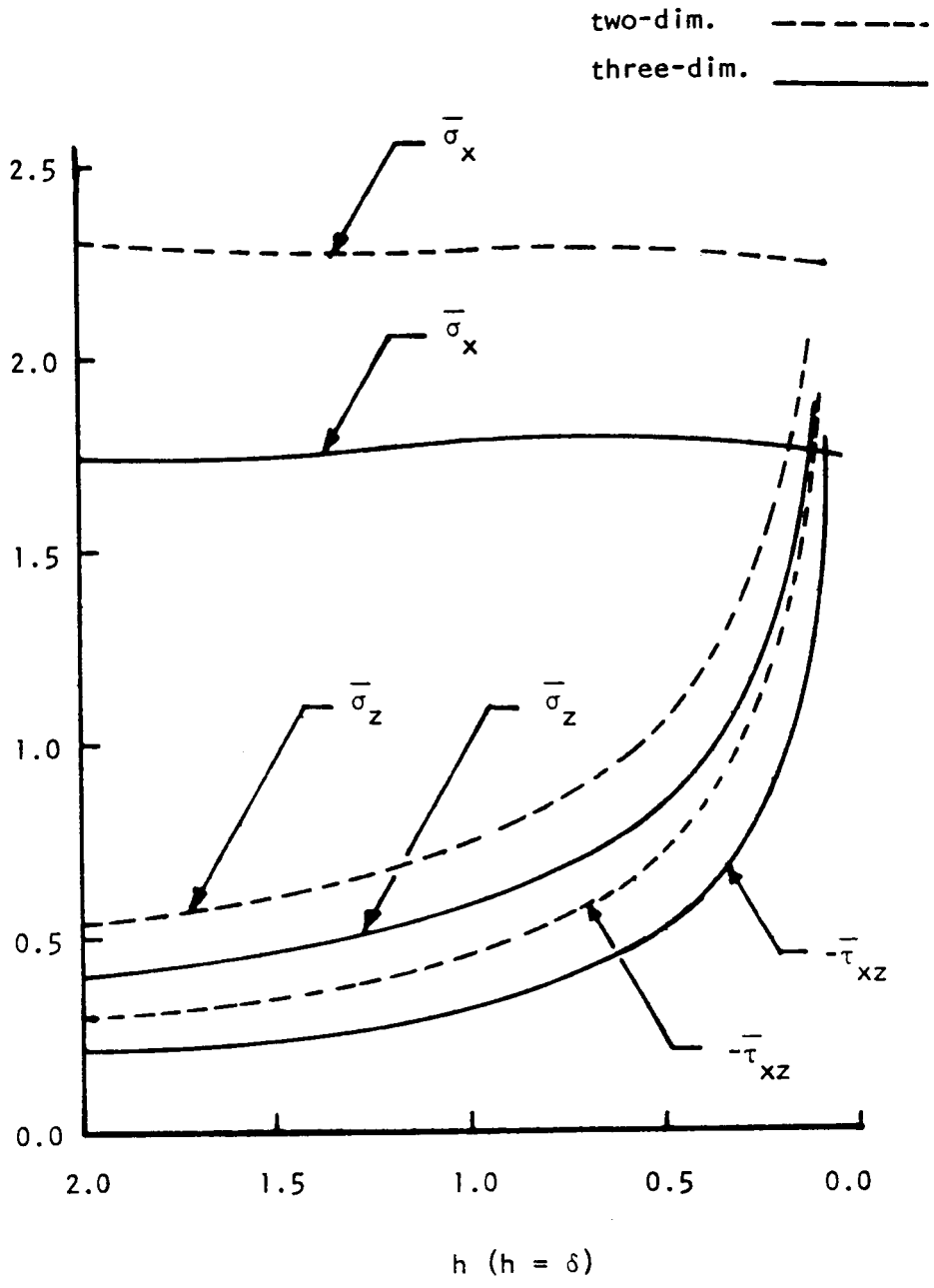

FIGURE 8. Maximum stresses as a function of fiber spacing for the present solution and [18], using case II of Figures 6 and 7. Square array of twenty-five broken fibers (five in the two-dimensional problem).

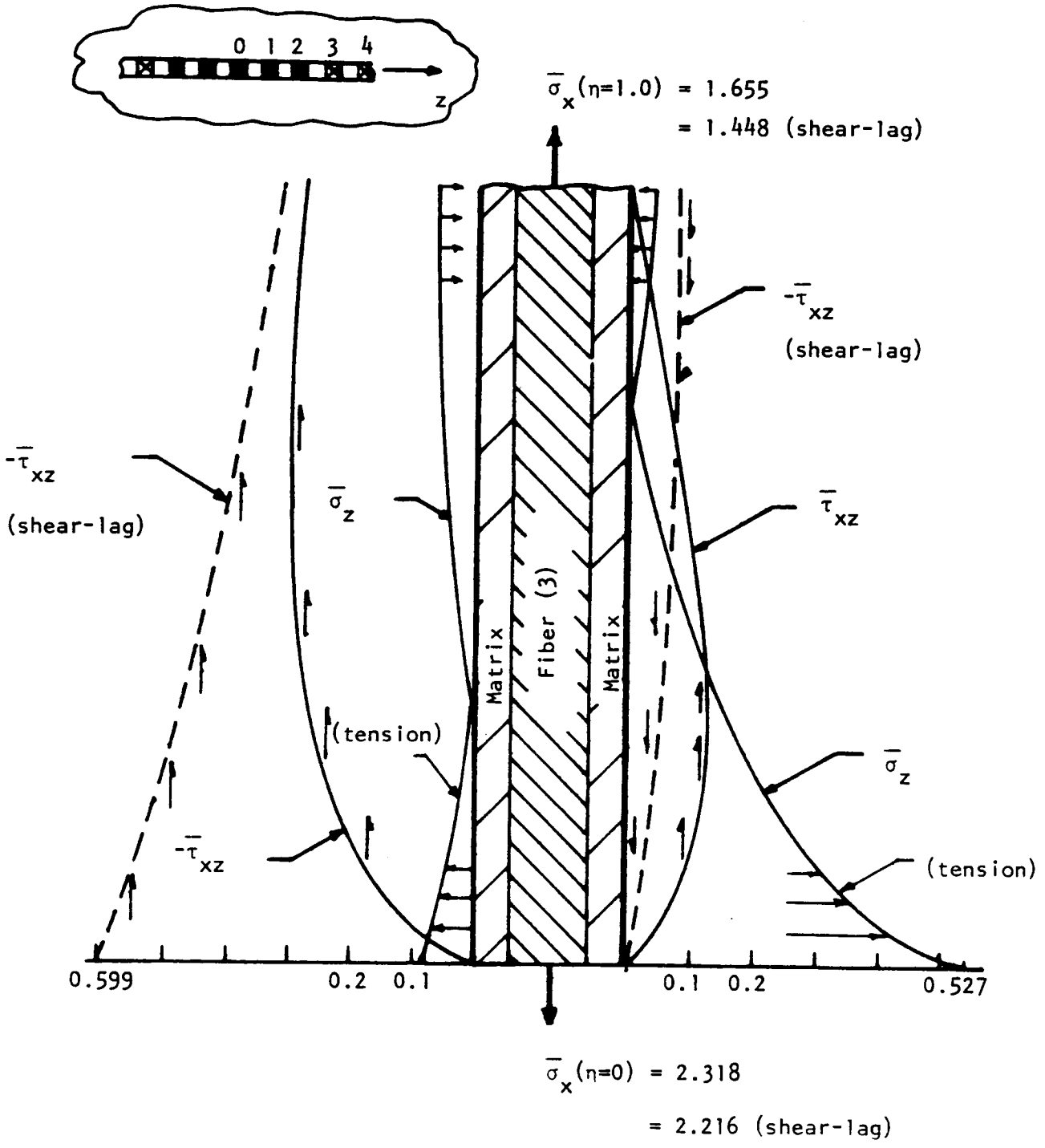

FIGURE 9. Stresses on the first intact fiber (3) for five broken fibers, two-dimensional solution, [18], h = δ = 2.0, γ = 0.5.

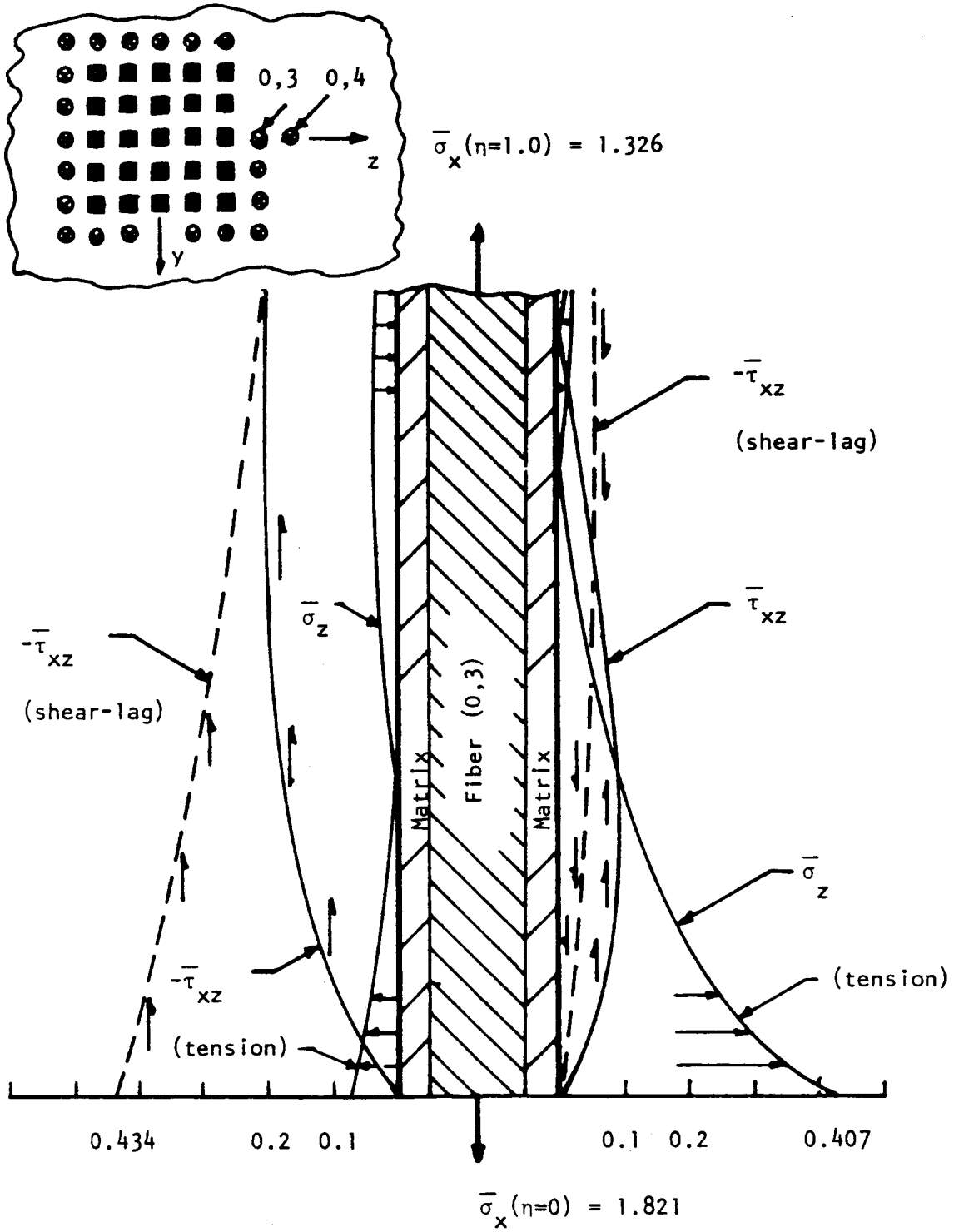

FIGURE 10. Stresses on the first intact fiber (0,3) for a square array of twenty-five broken fibers, present solution, $h = \delta = 2.0$, $\gamma = 0.5$.

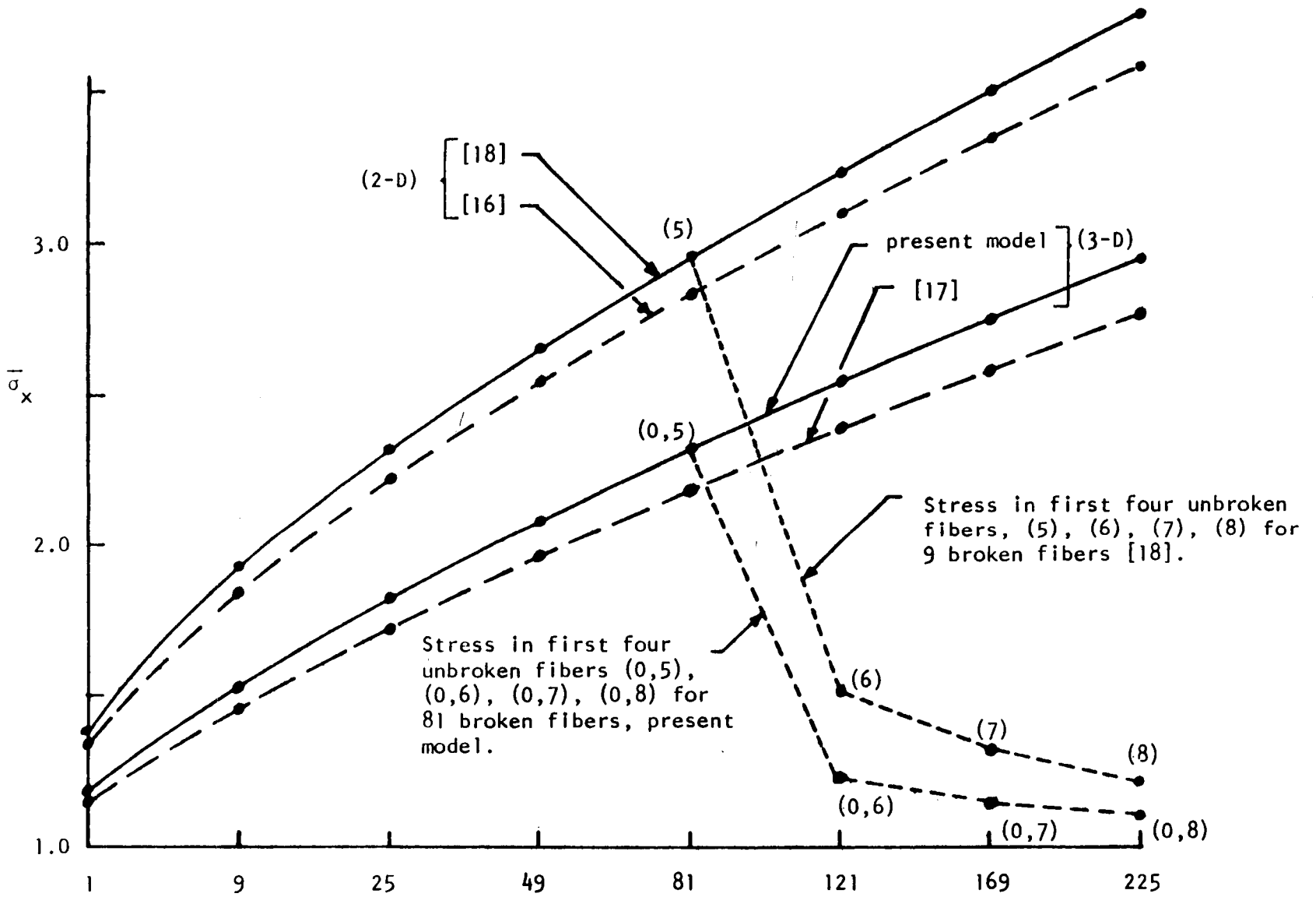

FIGURE 11. Fiber stress for a square array of broken fibers compared with [16], [17], and [18], $h = \delta = 2.0$, $\gamma = 0.5$.